

# Resistance to Fracture and Fatigue Crack Growth in Ni<sub>3</sub>Al Phase Based Intermetallic Alloy

L. Śniezek<sup>1</sup>, Z. Bojar<sup>2</sup> and P. Józwik<sup>1</sup>

<sup>1</sup> Military University of Technology, Institute of Machinery Construction

<sup>2</sup> Military University of Technology, Institute of Materials Technology and Applied Mechanics

**ABSTRACT:** Resistance to fracture and fatigue crack growth in Ni<sub>3</sub>Al intermetallic alloy with the alloying additions of Cr, Zr, and B was investigated. The specimens were subjected to cyclic three-point bending at R=0.1. Fatigue tests were preceded making the analyses both of the structures and the microhardness of materials. Several plots of crack length increments and crack growth rates against the range of stress intensity factor were presented. Examinations of the specimen fractures made with the help of both a SEM and an optical microscopes revealed a cleavage-like nature of fracture that have related to the material structure.

## INTRODUCTION

Low density, high ultimate strength and oxidation-resistance make the intermetallics an attractive and alternative materials applied for machine components manufacturing and working at an elevated temperature and/or in corrosion environment. There is, however, only a limited literature on fatigue cracking process developed in intermetallics, in particularly related to the Ni<sub>3</sub>Al phase based intermetallic alloys. A review of the works issued in 1990-1997 has been made by Stoloff [1]. The authors of those works have emphasized a very low resistance to fatigue cracking that is characteristic for most part of intermetallics. Crack initiation and propagation in these materials are mostly affected by many factors like: chemical composition, microstructure, temperature, and environmental conditions of the fatigue tests carried out. Very rapid growth of fatigue crack in the intermetallics has also been confirmed in [2 - 3]. In spite of a great interest of intermetallics including the Ni-Al system only few works of this issue is referred to the material under examination. The works [4, 5] prove that the cracking process runs slower in Ni<sub>3</sub>Al-based intermetallic alloys than in other ones. The differences were found to be greater at higher temperature [5]. The effects of crystallographic orientation of single crystal and polycrystalline intermetallic, type of loading and fatigue crack initiation and propagation were also studied. The Ni<sub>3</sub>Al intermetallic with the alloying additions Cr, Zn and B in the form of single crystal was investigated in [6].

It was found that crack initiation and growth depend on both the crystal orientation and the loading mode applied.

The aim of the paper is the research into the resistance to fracture and fatigue crack growth in the Ni<sub>3</sub>Al phase based intermetallic alloy under cyclic three-point bending at R=0.1.

## THE MATERIAL UNDER EXAMINATION

The Ni<sub>3</sub>Al-based intermetallic alloy was the material under investigations. The material was produced by applying step-by-step alloy melting in the inductive vacuum furnace of the Balzers type. In the first stage the master alloy, on the basis of elements Ni and Cr, was melted in vacuum. The second stage consisted in addition of aluminium and zirconium, whereas the third one - in remelting and correction of the chemical composition. Specimens in the final form of plates and cylinders were received as a result of casting in the malachite moulds. The chemical composition of obtained alloy is given in Table 1 whereas mechanical properties is collected in Table 2, respectively.

TABLE 1: Chemical composition of the Ni<sub>3</sub>Al-based (Cr-Zr-B) intermetallic alloy

Element (mass fraction)				
Al	Cr	Zr	B	Ni
11.5	7.5	0.73	0.04	balance

TABLE 2: Static strength properties of the Ni<sub>3</sub>Al-based (Cr-Zr-B) intermetallic alloy in as cast condition

Yield stress R <sub>0.2</sub>	Ultimate strength R <sub>m</sub>	Elongation A <sub>5</sub>	Reduction of area Z
[MPa]	[MPa]	[%]	[%]
516±9	597±8	0.8±0.2	0.6±0.2

## STRUCTURE AND MICRO-HARDNESS

The microstructure of the material revealed by a SEM microscope using the BSE method consisted of the following phases:

- the matrix:  $\gamma'$  (Ni<sub>3</sub>Al) phase - light-shadowed area (sign '1' in Fig. 1);
- the  $\gamma'$  (Ni<sub>3</sub>Al) +  $\beta$  (NiAl) intermetallic phases mixture - dark-shadowed area (sign '2' in Fig. 1);
- the  $\gamma'$  (Ni<sub>3</sub>Al) +  $\gamma'_{Cr}$  (considerably enriched by chromium) phase mixture - tiny grey precipitates area (sign '3' in Fig. 1).

The diversification of the alloy structure marks strongly as the microhardness of patterns is measured on the surface. The results of microhardness measurement for the selected microstructural phases are shown in Figure 2.

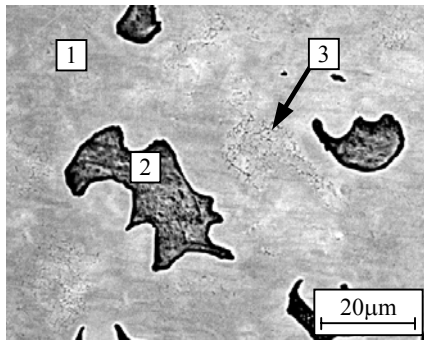


**Figure 1:** The Ni<sub>3</sub>Al (Cr, Zr, B) intermetallic alloy microstructure in as cast condition

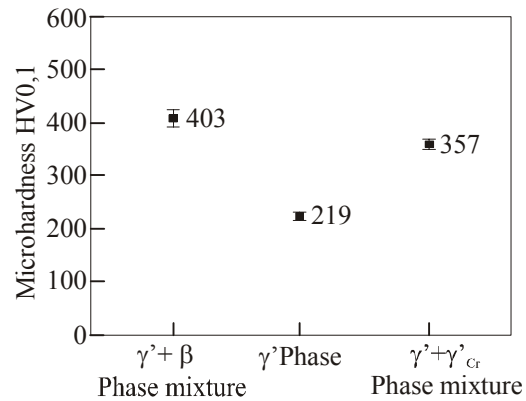


**Figure 2:** Microhardness of individual microstructural phases in Ni<sub>3</sub>Al (Cr, Zr, B) alloy

### SHARP-NOTCH TENSION TEST

Cylindrical notch-free and notched specimens (Figures 3a and 3b, respectively) were tested under axial-tension conditions.

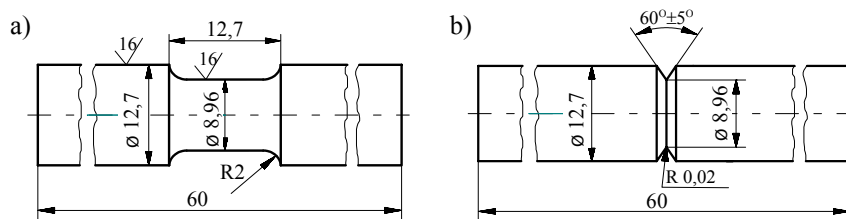


**Figure 3:** Specimens for the resistance-to-fracture tests

The goal of the sharp-notch tension test is to determine both a comparative resistance to fracture  $K$  of a thick-section under plane-strain conditions originating from a very sharp stress-concentrator and sharp-notch tensile strength of a specimen of given dimensions. Tensile strength depends on the size of specimens and mechanical properties of the material. The ratio of sharp-notch strength to yield stress is also calculated.

The stress-strain diagrams obtained for both notched and notch-free specimens enabled to determine the comparative resistance to fracture  $K$  as follows:

$$K = \frac{\sigma_s}{R_{0.2}} \quad (1)$$

where:  $\sigma_s$  means tensile strength of sharp-notch specimens and  $R_{0.2}$  is tensile yield stress of notch-free specimen.

Substituting the values of  $\sigma_s = 781 \pm 15$  MPa and  $R_{0.2} = 516 \pm 9$  MPa into Eq.1 we get:  $K = 1.51 \pm 0,08$

## FATIGUE CRACK PROPAGATION

The fatigue crack propagation tests were carried out at three-point bending for the edge-notched specimens of dimensions shown in Figure 4.

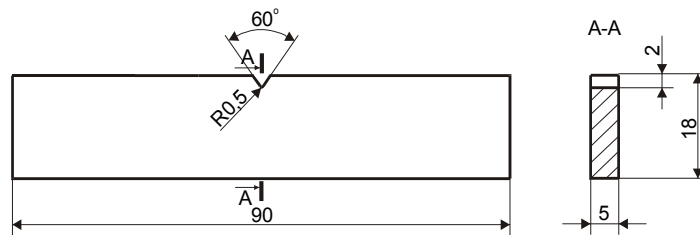


**Figure 4:** Geometry of specimen; dimensions in mm

Fatigue crack growth was monitored at the stress amplitude of values 150, 175, and 200 MPa, below the yield stress of material, using the replication method. The tests were conducted in air, at room temperature and at the frequency of loading 25 Hz. Current crack length  $l_i$  emanated at the notch root was measured after  $N_i$  number of loading cycles.

The structure of the alloy under investigation considerably affected the initiation and propagation of fatigue cracks. Figure 5a presents an exemplary image of two cracks propagated in the specimen after  $N=8.2 \cdot 10^5$  cycles at the stress amplitude  $\sigma_a=150$  MPa. Crack '1' propagates from the bottom of the edged notch. After  $N=5.65 \cdot 10^5$  cycles the crack was found to be arrested. After that the crack '2' become visible in the area under observation. The source of this crack was found to be inside the specimen, in a distance of 0.6 mm away from the notch root. At higher magnification

of the image a bridge which joins the propagating cracks '1' and '2' can be revealed (Figure 5b). Variation in the stress amplitude  $\sigma_a$  did not affect considerably the paths of the propagated cracks where jogs, slow-downs, and local changes in the direction of propagation can be selected.

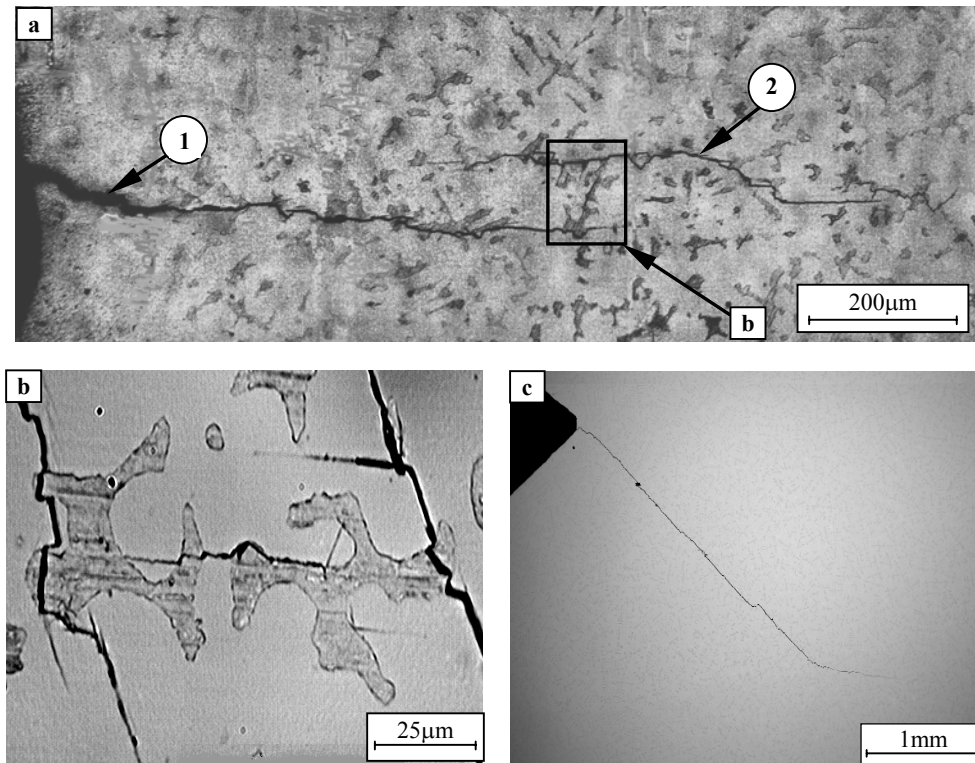


**Figure 5:** Image of fatigue crack advanced in the  $\text{Ni}_3\text{Al}$  (Cr, Zr, B) intermetallic alloy (*a,b*:  $\sigma_a = 150 \text{ MPa}$ ,  $N = 8.2 \cdot 10^5$ , *c*:  $\sigma_a = 175 \text{ MPa}$ ,  $N = 4.4 \cdot 10^5$ ); explanations in the text.

In several specimens the fatigue cracks were observed to propagate from the root of the notch at the angles a round of  $25 - 40^\circ$  to the specimen cross-section whereas on the opposite surface of the specimen the cracks advanced in a direction resulted from the applied type of loading. Figure 5c exemplifies such cracking in the specimen tested at  $\sigma_a = 175 \text{ MPa}$  after the  $N = 4.4 \cdot 10^5$  number of cycles.

## FATIGUE CRACK GROWTH RATE

On the basis of experimental results the courses of crack length increments  $l$  against the cycle ratio  $N_i/N_f$  and the crack growth rates  $dl/dN$  versus  $\Delta K$  have been plotted on Figure 6a, and 6b, respectively. The range of stress intensity  $\Delta K$  was calculated according to equation 2 [7]:

$$\Delta K = 1.1215 \cdot k_t \cdot \Delta\sigma \cdot \sqrt{\pi \cdot l} \quad (2)$$

where:  $k_t$  means stress concentration factor,  $\Delta\sigma = 2 \cdot \sigma_a$  - stress range and  $l$  denotes crack length.

The plots in diagrams prove a great irregularity of fatigue crack growth rates that is resulted from a multiphase structure of the material, big scatter of the size of the adjacent grains and different crystallographic orientation of the polycrystalline material. Because of growth rates discontinuity those rates can be calculated only in separate intervals of the width of the specimens and any comparative analysis of the curves is more difficult. Significant differences in fatigue-crack growth rates noted for various stress amplitudes  $\sigma_a$  became extremely evident at lower values of  $\Delta K$  ( $<40 \text{ MPa}\sqrt{\text{m}}$ ).

## MORPHOLOGY OF FATIGUE FRACTURE SURFACES

The microfracture analyses made with the help of a scanning electron microscope revealed the details of microstructure, morphology and mechanism of fracture proper the distinguished area of the fracture surfaces of the specimens. The image in Figures 7a is originated from fatigue zone of whereas the image in Figure 7b.- from the region of final fracture. The specimen was examined at  $\sigma_a=175 \text{ MPa}$ , cycles to failure  $N_f=5.98 \cdot 10^5$ . What was observed here is the brittle transcrystalline fracture in fatigue region accompanied with the above-mentioned jogs of crack growth rates. Brittle fracture along the crystallite boundaries is a predominant phenomenon in the region of a final fracture. The brittle fracture runs at high rate, the fact being manifested by numerous fracture-originated cracks and, here and there, cleavage fractures along the cleavage planes (Figure 7b).

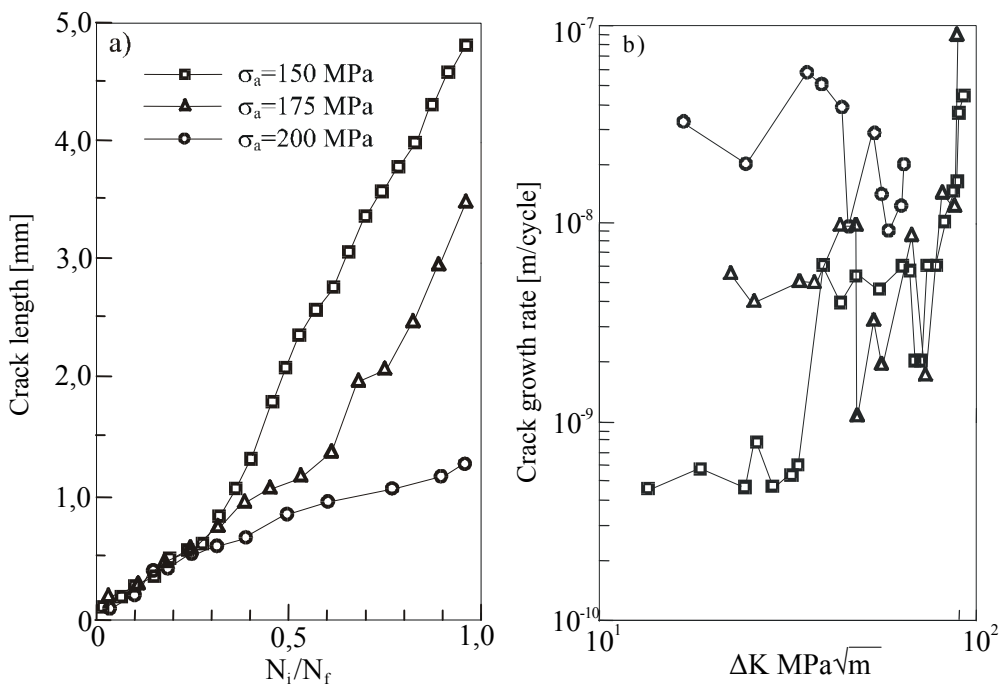


**Figure 6:** The crack growth rates for the Ni<sub>3</sub>Al intermetallic alloy with the alloying additions of Cr, Zr, and B; a)  $l_i=f(N_i/N_f)$ , b)  $dl/dN=f(\Delta K)$ .

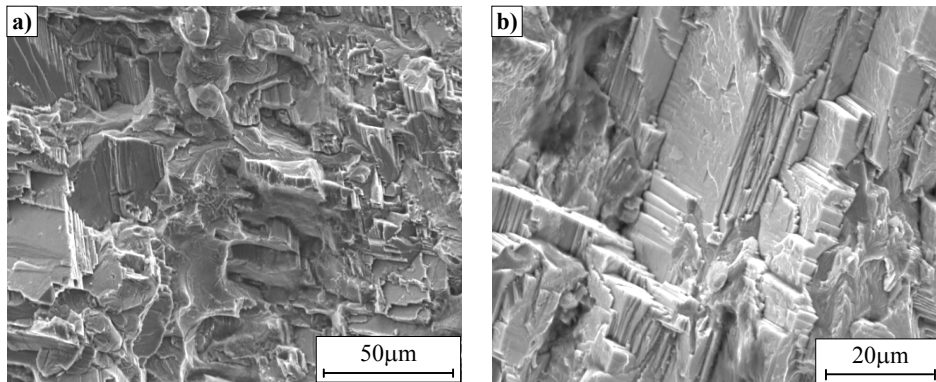


**Figure 7:** Microstructure of fatigue fracture surfaces within the Ni<sub>3</sub>Al intermetallic alloy with the alloying additions of Cr, Zr, and B: a) - the fatigue region; b) - the region of the final fracture.

## CONCLUSIONS

The above-presented results of resistant to fracture, crack growth rate and mechanism of cracking are referred to a selected as-cast alloy based on the intermetallic phase  $Ni_3Al$  with the alloying additions of Cr, Zr, and B. They prove an irregular mode of fatigue crack propagation to be affected by the numerous factors as: complex dendritic multiphase structure of the alloy and big scatter of the size of the adjacent grains. Both the direction and the local rate of fatigue crack growth strongly depend on crystallographic grain orientations. The tests have also confirmed the results presented in [1]. A very complex cracking mechanism has been reflected by the electron and optical examination of fracture surfaces. Transcrystalline fracture with numerous jogs affected by the crack's snapping-through from one cleavage plane to another. The cracking along the crystal-grain boundaries with local symptoms of cleavage fracture was found in the final-fracture region.

## REFERENCES

- [1] Stoloff N. S., (1997) Fatigue crack growth in intermetallics, *Structural Intermetallics*, 33-42.
- [2] Chen W. Z. i inni, (1999) *Fatigue crack growth in Ti-48al.-2Mn-2Nb alloy produced by centrifugal spray desposition*. International Fatigue Congress, 8-12 June, Beijing, P. R. China, pp.1579-1584.
- [3] Reji J. i inni, (1999) *Mixed mode crack growth in a gamma titanium aluminide*. International Fatigue Congress, 8-12 June, Beijing, P. R. China, pp.1567-1572.
- [4] Zhang G. P., and Wang Z. G. (1999) *Influence of loading waveform on high temperature creep-fatigue crack growth of  $Ni_3Al$  alloys*. International Fatigue Congress, 8-12 June, Beijing, P. R. China, pp.1621-1626.
- [5] Stoloff N. S. i inni, (1987) *High Temperature Ordered Intermetallic Alloys II*, Eds, Mat. Res. Soc. Symp. Proc. 81, Pittsburgh, PA, MRS, pp.247-261.
- [6] Zhang G.P., and Wang Z.G. (1997) *Mode I and Mixed mode I/II fatigue cracking in  $Ni_3Al(CrB)$  single crystals*. Fatigue Fracture Engng. Mater. Struct. Vol.20, 6, pp.883-894.

- [7] Xu R. X., Topper T. H., Thompson J. C., (1997) *Mode I Stress Intensity Factor Equations for Cracks at Notches and Cavities*. Fatigue Fracture Engng Mater. Struct. Vol. 20, No. 9, pp.1351-1361.